Performance of an Imaging Shack-Hartmann Wavefront Sensor for Space Domain Awareness Observations

Daniel Johns, Douglas A. Hope, Stuart M. Jefferies,
Fabien R. Baron and Dmitriy Shcherbik
Georgia State University

ABSTRACT

Imaging Shack-Hartmann Wavefront Sensor (ISH-WFS) data, when analyzed as a time-series in post-processing, serve as powerful tools to image objects in space with unprecedented accuracy, and allow for studies to be done on atmospheric statistics. Here we evaluate the performance of an ISH-WFS for tomographic recovery of the atmosphere and recovery of objects for Space Domain Awareness (SDA). We probe a wide range of narrow-band photometric magnitudes, varying degrees of turbulence, and point and extended sources. Separation of layers is made possible by assuming the atmospheric layers translate across the aperture of the telescope due to winds, and the extension to a full tomographic solution requires detectable anisoplanatic effects in the image. This means that tomography is not possible for narrow fields of view, however layer separation is still possible and provides improved wavefront and object estimates. For this, wind speed and direction must be known during reconstruction. We show that these can be retrieved from the ISH-WFS data using a 3D autocorrelation technique but only if the number of sub-apertures allows for fine enough sampling of the atmosphere. Here we find that 6 sub-apertures across the pupil are sufficient to extract all of the necessary wind parameters for layer separation down to a brightness of $m_V = 14$. Finally, we discuss the potential performance gains by expanding the ISH-WFS to observe over the full sensitivity range of a typical silicon detector ($400 - 1000$ nm).

BACKGROUND

High-resolution, high-contrast imaging of resident space objects (RSOs) represents a cornerstone of Space Domain Awareness (SDA). Achieving this capability requires accurate estimation of the complex wavefront, which carries information about reflected light from RSOs. Turbulence in the atmosphere causes random fluctuations in both the wavefront phase and intensity, and thus accurate modeling of the complex wavefront is required.

Scene-based (or "imaging") Shack-Hartmann Wavefront sensors (ISH-WFS) have been utilized in solar physics on a frame-by-frame basis to drive adaptive optics. They differ from the traditional SH-WFS, where each sub-aperture image is sampled by 2x2 or 3x3 pixels, by sampling the sub-aperture images with a greater number of pixels (typically ≥ 20) such that a low spatial resolution image is formed. When analyzing a time-series of ISH-WFS frames in post-processing, and leveraging temporal correlations in the atmosphere, wavefront estimates with low root-mean-square error (RMSE) values can be achieved. By allowing for temporal correlations in the wavefront, via the frozen flow hypothesis, it is possible to separate the different atmospheric layers, providing a valuable reduction in recovered wavefront RMSE [4]. If the data are treated with an isoplanatic imaging model when anisoplanatic effects are present then the recovered point-spread functions (PSFs) will suffer from a lose of accuracy towards the edges of the image. However, [6] showed that anisoplanatic effects allow the separate layers to be placed at their respective heights, providing additional reductions in the recovered wavefront RMSE, and more faithful PSFs across the entire image.

These factors make the ISH-WFS a powerful tool for accurate recovery of wavefronts and objects. However, its performance in a Speckle imaging framework has yet to be benchmarked properly. Here, we subject the ISH-WFS to a variety of turbulence strengths and beacon brightness and assess the fidelity of the recovered wavefronts. Additionally, we test the ability of the ISH-WFS to extract wind velocities of atmospheric layers. Finally, we discuss extensions of the ISH-WFS to the broadband and the implications that come with imaging across a wide passband.

METHODS

Multi-Frame Blind Deconvolution

For object estimation and atmospheric phase recovery from data augmented with SH- or ISH-WFS data we use a Multi-Frame Blind Deconvolution (MFBD; [2]) algorithm. A sufficient starting point for the object estimate is the average of all the frames, which we then use to solve for the phase. Initial estimates of the PSFs are obtained from the WFS slopes and the object is estimated using these. Then, an alternating minimization is performed between the phase and object estimations. This alternating minimization approach is iterated until convergence is reached and helps to avoid entrapment in local minima.

We minimize the discrepancy between each observed and synthetic image for a time series of full-aperture and ISH-WFS frames. The n-th model image in a sequence of N_{frames} is represented as a convolution of the estimated object (f) with the frame's point-spread function (h_n; PSF). Furthermore, the PSF is estimated using Fourier optics as $h_n = FT^{-1}[P_n \star P_n]$, where $\star$ is the correlation, FT^{-1} is the inverse Fourier transform, and P_n is the Pupil function given by $P_n = A_n \cdot \exp i\phi_n$. By modeling the PSFs in the Fourier domain in this way and assuming Nyquist sampling we reduce the number of variables from $N_{frames} \cdot N_{pix}^2$ in the image domain, where N_{pix} is the number of pixels along one side of the image, to $N_{frames} \cdot N_{pix}^2/2$ in the Fourier domain. We further assume the amplitude variations to be negligible, reducing the amount of variables needed to describe the atmospheric phase (and therefore the PSFs) to $N_{frames} \cdot N_{pix}^2/4$. By utilizing the frozen flow we can greatly reduce the number of variables by introducing correlation in the phase from one frame to the next and reconstructing the phase on a continuous "sausage" rather than individually per frame. The orientations and lengths of the phase sausages are determined by each layer's wind velocity, which must be known prior to reconstruction. How we determine the layer's wind velocity is described in further detail below.

Numerical Simulations

We simulate a 3.6 m telescope equipped with a 6x6 ISH-WFS. To compare to a traditional SH-WFS we also simulate a 32x32 sub-aperture array under the same conditions outlined below. In both cases a set of full-aperture images was synthesized to supplement the WFS data. The atmospheric conditions corrupting the observations are described with a power spectrum exhibiting Kolmogorov statistics [5]. Two atmospheric layers were considered: one ground layer and one high-altitude layer, both of which are assumed to obey the frozen flow hypothesis. The strengths of these layers ranged from $r_0 = 9 - 72$ cm, corresponding to $D/r_0 = 5 - 40$. Observations are assumed to be over a narrow field-of-view and across a narrow bandpass ($\Delta\lambda = 90$ nm at 550 nm), therefore allowing us to use an isoplantic imaging model and ignore chromatic effects. Finally, we simulate observations of a constellation of 5 laser guide stars (LGS) of brightness $m_V = 7$[1]. An example of the full-aperture images for the LGS constellation is seen in Fig. 1 at a range of D/r_0 values.

Extracting Wind Velocity from WFS data

Accurate knowledge of the wind velocity of each atmospheric layer is crucial to provide the highest-fidelity reconstructions under the frozen flow assumption. First, we tested the capabilities of the ISH-WFS when each sub-aperture image is binned to 2x2 pixels, effectively creating a traditional SH-WFS. The downside of this approach is that the binning of pixels causes the read noise to be combined, reducing the final SNR when compared to a SH-WFS. Wind velocities were extracted using a 3D auto-correlation technique where we first calculate the centroid in each sub-aperture for each frame in the time series. Then, this time-series of centroids is 3D auto-correlated and the wind velocity of each layer is extracted from the auto-correlation function peaks.

For this test we simulate observations with a 3.6 m telescope through a single atmospheric layer with $r_0 = 18$ cm ($D/r_0 = 20$), wind speed $|V| = 13.6$ m/s, and wind direction $\theta = -26.4^{\circ}$[2]. We then tested the effectiveness of our wind velocity extraction method at different source brightness, $m_V = 10, 12, 14, 16$, and with different sub-aperture configurations: 6x6, 8x8, 10x10, and 12x12. The results of this analysis can be found in Table 1 and are discussed in detail below.

[1] $m_V = 7$ is typical of a Sodium laser operated at 10W.

[2] Here we define East to be $\theta = 0$, increasing counterclockwise.

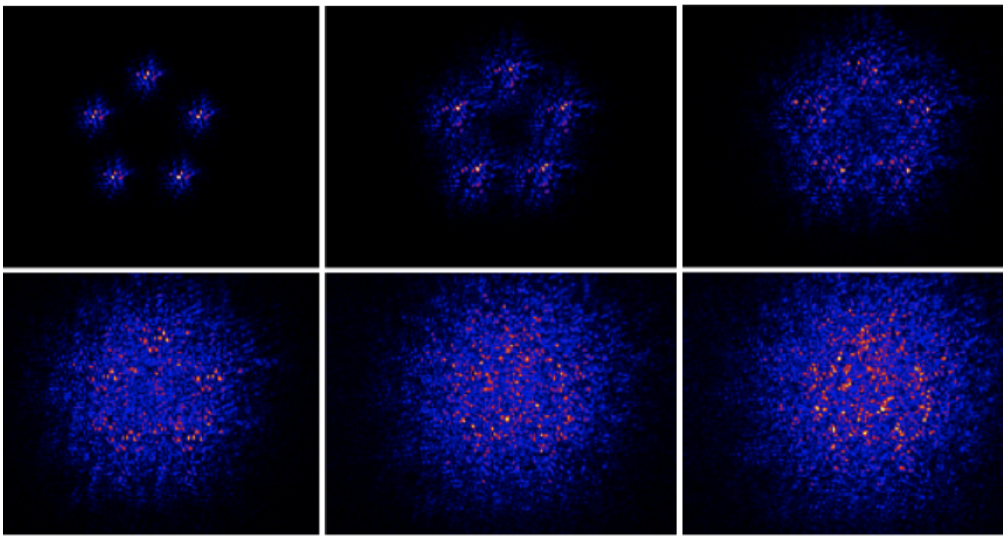

Fig. 1: Full image data of the LGS constellation at turbulence levels of $D/r_0 = 5$, 10, 15, 20, 25, and 30 from top left to bottom right.

RESULTS & DISCUSSION

Wind Velocity Extraction

The results of our wind velocity extraction method are shown in Table 1. For a single layer we found that for beacons brighter than $m_V = +12$ all of the ISH-WFS configurations were capable of extracting wind speeds to within 3% and directions to within 15% of the truth value. At $m_V = 14$ both the 10x10 and 12x12 configurations failed to extract wind velocities due to insufficient SNR in the sub-aperture images. For beacons fainter than $m_V = +14$ none of the configurations had sufficient SNR to extract wind velocities.

		Single Layer ($\|V\| = 13.6$ m/s, $\theta = -26.4°$)	
m_V (mag)	Config. (NxN)	Wind Speed $\|V\|$ (m/s)	Wind Direction θ (deg; East = 0)
10	6x6	13.9	-22.3
	8x8	14.0	-23.5
	10x10	13.8	-27.5
	12x12	13.7	-25.8
12	6x6	13.9	-22.3
	8x8	13.7	-28.1
	10x10	13.8	-27.5
	12x12	13.7	-25.8
14	6x6	13.9	-22.3
	8x8	13.7	-28.1
	10x10	-	-
	12x12	-	-

Table 1: Recovered Wind velocities for the case of an ISH-WFS binned to 2x2 pixels, and a truth wind speed of $|v| = 13.6$ m/s and direction $\theta = -26.4°$. At $m_V = 14$ both the 10x10 and 12x12 lacked sufficient SNR to extract wind velocities, and at $m_V > 14$ all of the configurations failed to recover velocities.

Turbulence Strength

For the LGS constellation the residual wavefront RMSE can be seen in Fig. 2 as a function of D/r_0 for a SH-WFS, SH-WFS with frozen flow, ISH-WFS with frozen flow, and ISH-WFS supplemented with full-aperture images. From this it is clear that the frozen flow hypothesis brings with it significant performance gains. However, the most significant gain comes from the use of an ISH-WFS over the traditional SH-WFS. Not only is the wavefront RMSE significantly reduced in all cases, but at high turbulence values the reconstructions provide unprecedented RMSE. This is significant because it opens the window of observation to more severe conditions, allows for observations at low Zenith angles (closer to horizon), and has implications for larger diameter telescopes where the apparent effects of turbulence become amplified.

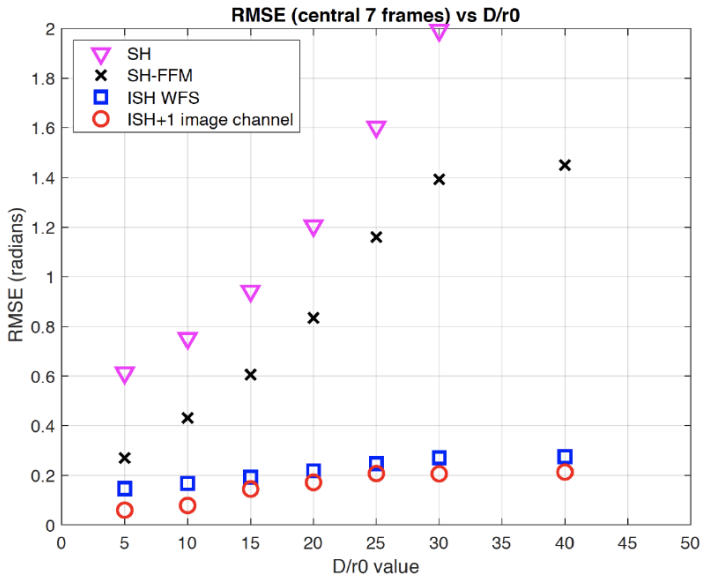

Fig. 2: Wavefront RMSE as a function of turbulence strength for the constellation of LGS. (pink inverted triangles) traditional SH-WFS, (black x's) SH-WFS under the frozen flow hypothesis, (blue squares) ISH-WFS under the frozen flow hypothesis, (red circles) ISH-WFS and full-aperture imaging channel. Note the reduction in RMSE in the ISH-WFS reconstructions at high D/r_0 values.

These recovered phases contain physically meaningful information on the atmosphere. When coupled with wind velocity information they serve as an important resource for further studies on atmospheric statistics.

FUTURE WORK

Opportunities for further refinement in the wavefront recovery algorithm are endless. For example, currently the MFBD algorithm assumes negligible amplitude variations over the pupil. This assumption, though sufficient for many cases, needs to be relaxed in order to provide the highest fidelity reconstructions where both pristine spatial frequency and photometric recovery are required, such as in the case of high-contrast and closely-spaced objects.

Numerical simulations show that we require beacons at least as bright as $m_V = +12$ when using a 3.6 m telescope. This is brighter than for other types of WFS (e.g., curvature based sensors). To gain sensitivity, rather than increase the exposure time and lose the temporal correlations, which preserve high spatial frequency information in the wavefront, we propose to extend the ISH-WFS to a broad spectral region (500 nm or more). The extension to the broadband brings with it additional effects, notably chromatic dispersion. This effect, however, means the high-altitude atmospheric layers are sampled differently according to wavelength. Sampling the upper atmosphere differently serves to improve the tomographic reconstruction further. By opening up the spectral bandwidth available to the ISH-WFS we collect four times more photons than through a V-band filter (FWHM $\sim$ 90 nm), but then the challenge becomes estimating the spectral dependence of the RSO intensity distribution and the time-varying atmospheric PSF. Recent

work has shown that hyperspectral imaging across a broad spectral range can successfully recover the spectrum of the target by modeling the PSF and object simultaneously at narrow wavelength regions across the entire bandpass [1]. The performance gains from hyperspectral imaging will allow for observations at lower Zenith angles, but more importantly, it will allow for improved detection and characterization of RSOs through the recovery of spectral information on the target. The current work of [3] demonstrates the proof of concept on both a toy satellite and toy binary star system that recovery of spectral information is possible with broadband observations. This is particularly useful for studying the characteristics of aged materials in space.

The ISH-WFS can also be used in real time to drive an AO system, while also collecting WFS data for the post-processing techniques outlined above. These data contain information on the residual wavefront after AO compensation. When reconstructed with the MFBD algorithm the reconstructed wavefronts should achieve even lower wavefront RMSE than seen in this work. It is noted, however, that using an ISH-WFS in this way breaks the physical meaningfulness in the recovered phases, which would serve solely as a means to estimate accurate PSFs.

ACKNOWLEDGEMENTS

This material is based upon work supported by the Air Force Office of Scientific Research under award number FA9550-21-1038. Any opinions, findings, conclusions, or recommendations expressed in this material are those of the authors and do not necessarily reflect the views of the United States Air Force.

[1] Ryan Hall and Stuart M. Jefferies. Hyper-spectral speckle imaging for space situational awareness. *The Journal of the Astronautical Sciences*, 69(2):581–592, Apr 2022.

[2] Douglas A. Hope, Stuart M. Jefferies, Michael Hart, and James G. Nagy. High-resolution speckle imaging through strong atmospheric turbulence. *Opt. Express*, 24(11):12116–12129, May 2016.

[3] Stuart Jefferies, Ryan Hall, Fabien Baron, Daniel Johns, Dmitriy Scherbik, and Douglas Hope. Hyper-Spectral Speckle Imaging of Resolved Targets. In *The Advanced Maui Optical and Space Surveillance Technologies Conference*, September 2023.

[4] Stuart M. Jefferies and Michael Hart. Deconvolution from wave front sensing using the frozen flow hypothesis. *Optics Express*, 19(3):1975–1984, January 2011.

[5] R G Lane, A Glindemann, and J C Dainty. Simulation of a kolmogorov phase screen. *Waves in Random Media*, 2(3):209–224, 1992.

[6] Matthew Willson, Stuart Jefferies, and Douglas Hope. Tomographic Wave Front Sensing using an Imaging Shack-Hartmann Wave Front Sensor and Multi-Frame Blind Deconvolution. In S. Ryan, editor, *The Advanced Maui Optical and Space Surveillance Technologies Conference*, page 70, September 2018.